Journal of ELECTRONIC MATERIALS, Vol. 45, No. 8, 2016
DOI: 10.1007/s11664-016-4589-z

Dielectric Properties and Complex Impedance Analysis of BT–BMT–BS Ceramics

RAZ MUHAMMAD,[1,2,4] AMIR KHESRO,[2] and MUHAMMAD UZAIR[3]

1.—Department of Physics, Islamia College University, Peshawar 25120, KP, Pakistan. 2.—Department of Materials Science and Engineering, University of Sheffield, Sheffield S1 3JD, UK. 3.—Department of Physics, University of Peshawar, Peshawar 25120, KP, Pakistan. 4.—e-mail: razmohammad_phy@yahoo.com

Polycrystalline $(1-x)BaTiO_3$–$0.5xBi(Mg_{0.5}Ti_{0.5})O_3$–$0.5xBiScO_3$ (x = 0.4, 0.45, 0.5, and 0.55) samples have been prepared via a conventional mixed-oxide solid-state sintering route. Phase analysis of the samples with $x \geq 0.45$ revealed formation of single-phase cubic structure, while at x = 0.4, a minor secondary phase formed. Complex impedance spectroscopy of the samples revealed more than one type of transport mechanism (grain/bulk, grain boundary, and electrode effect). At x = 0.4, the grain boundary was less conducting than the grain; however, grains dominated the total conductivity with further increase in x. At elevated temperatures, the higher conductivity values suggest semiconducting-like behavior with negative temperature coefficient of resistivity. The composition with x = 0.55 exhibited a temperature-stable relative permittivity (ε_r) of 1430 (±15% over 127°C to 500°C) and dielectric loss (tan δ) of <0.025 (over 150°C to 370°C).

Key words: Dielectric properties, $BaTiO_3$, impedance spectroscopy

INTRODUCTION

Capacitors are used for a variety of functions such as coupling, decoupling, filtering, and voltage smoothing in electronic circuits.[1] High relative permittivity (ε_r) is an important parameter for miniaturization of capacitors and hence electronic devices. $BaTiO_3$ (BT) has tetragonal structure at room temperature and exhibits high ε_r of ~10,000 at the ferro- to paraelectric phase transition (T_c) near 130°C. T_c occurs due to displacement of Ti^{4+} ion relative to oxygen octahedra caused by hybridization between Ti 3d and oxygen 2p states.[2] Doping BT has successfully produced temperature-stable capacitors operating in the range from −55°C to an upper limit of ~200°C.[3] However, many applications including deep oil and gas drilling, aircraft, and automotive vehicles demand capacitors to operate in still harsher environments with temperatures greater than 200°C.[4,5] The temperature stability in these ceramics is mostly observed for the pseudocubic/cubic phase(s).

Health and environmental effects of lead have increased the importance of BT-based systems. Like Pb^{2+}, Bi^{3+} possesses a lone pair of electrons which is not involved in chemical bonding but is highly polarizable, which helps to maintain high ε_r characteristics of the host compound.[2] In general, solid solutions of Bi-based and BT perovskites promote relaxor behavior to flatten the sharp ε_r peak of the conventional ferroelectric BT. Such flattening of the ε_r peak may be enhanced by compositional and structural inhomogeneities, e.g., core–shell structure, reported for BT–BS and $Na_{0.5}K_{0.5}TiO_3$–$LiTaO_3$–$BiScO_3$ ceramics.[6,7] Dittmer et al.[8] reported ε_r of ~2000 (±10%) at 1 kHz in the temperature range of 43°C to 319°C for the $Bi_{0.5}Na_{0.5}TiO_3$–$BaTiO_3$–$K_{0.5}Na_{0.5}NbO_3$ system. In this case, the flattening of the ε_r peak was correlated with the smearing of two distinct anomalies of the end members.[8] Similarly, other compounds of interest are $BaTiO_3$–$Bi(Mg_{0.5}Ti_{0.5})O_3$ (BT–BMT),[9,10] $BaTiO_3$–$Bi(Mg_{0.5}Zr_{0.5})O_3$ (BT–BMZ),[11] $BaTiO_3$–$Bi(Zn_{0.5}Ti_{0.5})O_3$ (BT–BZT),[6] $BaTiO_3$–

(Received January 23, 2016; accepted April 27, 2016; published online May 11, 2016)

$BiScO_3$ (BT–BS),[6] and $Ba_{0.8}Ca_{0.2}TiO_3$–$Bi(Mg_{0.5}Ti_{0.5})O_3$–$NaNbO_3$.[12] Substitution of Ba^{2+} by Bi^{3+} and of Ti^{4+} by trivalent Sc^{3+} ions has been used for charge compensation,[6,10] resulting in temperature-stable ε_r = 1000 from room temperature to 400°C. On the other hand, BT–BMT compound exhibited high ε_r = 2248 in the narrow temperature range of 238°C to 400°C. In the BT–BS system, ε_r is lower but the operating temperature range is wider than for BT–BMT. Also, Sc^{3+} is relatively more expansive, so the Sc^{3+} content can be decreased by partial replacement with $Mg_{0.5}Ti_{0.5}$, which may also increase ε_r. Furthermore, very few studies on complex impedance spectroscopy of these materials exist in literature. In the present study, we report the structure–property relation in $(1-x)BaTiO_3$–$0.5xBi(Mg_{0.5}Ti_{0.5})O_3$–$0.5xBiScO_3$ (BT–BMT–BS) solid solution using x-ray diffraction analysis, dielectric measurements, and impedance spectroscopy.

EXPERIMENTAL PROCEDURES

$(1-x)BaTiO_3$–$0.5xBi(Mg_{0.5}Ti_{0.5})O_3$–$0.5xBiScO_3$ (BT–BMT–BS) (x = 0.4, 0.45, 0.5, and 0.55) samples were prepared through a solid-state sintering route. Initial ingredients ($BaCO_3$, Bi_2O_3, TiO_2, MgO, and Sc_2O_3) were dried at 180°C prior to weighing. The raw materials were weighed according to the stoichiometric ratios and then mixed/milled in polyethylene milling jars for 12 h using isopropanol as lubricant and Y-toughened zirconia balls as milling medium. The mixed/milled powders were calcined at 925°C for 6 h in covered alumina crucible and then remilled using agate mortar to dissociate agglomerates (if any). The calcined powders were pressed into cylindrical pellets using an isostatic pellet press at 50 MPa and sintered at 1000°C to 1175°C for 4 h.

The density of the pellets was measured using a high-precision electronic densitometer (Mettler Toledo, Switzerland). Phase analysis was carried out using a D-5000 Siemens x-ray diffractometer operated at 40 kV and 30 mA, with Cu K_α radiation (λ = 1.54018 Å). Data were collected in the $20° \le 2\theta \le 70°$ range, with step size of 0.02° at 1.5 min/step. ε_r and tan δ at 1 kHz to 1 MHz were measured in the temperature range of ~25°C to 500°C, using a HP 4284A precision LCR meter with an applied alternating-current (ac) voltage of 100 mV. Impedance spectroscopy of these samples was carried out using an E4980A (Agilent) impedance analyzer in the frequency range from 20 Hz to 2 MHz.

RESULTS AND DISCUSSION

Figure 1 presents the x-ray diffraction patterns of the BT–BMT–BS samples sintered at 1150°C for 4 h. The Bragg reflections from all the sample matched PDF#01-073-6325 for cubic ($Pm\bar{3}m$) structure; however, an extra reflection was observed for the sample with x = 0.4, which could not be assigned and needs further investigation using transmission electron microscopy to determine the unknown phase and its distribution in the local structure. Bi^{3+} (1.03 Å < r_{Bi} < 1.61 Å) and Ba^{2+} (r_{Ba} = 1.61 Å) ions occupy the A-site, while Ti^{4+} (r_{Ti} = 0.605 Å), Mg^{2+} (r_{Mg} = 0.72 Å), and Sc^{3+} (r_{Sc} = 0.745 Å) ions occupy the B-site of the lattice.[13] The lattice parameters were calculated using the least-squares method, indicating a slight change from 4.0444 Å (for x = 0.4) to 4.0567 Å (for x = 0.55). The observed increase in lattice parameter with increase in x leads to an increase in the unit cell volume, which may be attributed to substitution of B-site cation (Mg^{2+} and Sc^{3+}). The B-site cations with larger ionic radii replacing Ti^{4+} with smaller ionic radius may increase the volume of BO_6 octahedra and hence the unit cell volume.[14]

The temperature dependence of the relative permittivity and loss tangent at different frequencies for the BT–BMT–BS samples is shown in Fig. 2a–d. The observed relaxor-like behavior may be due to relaxation of polar nanoregions arising due to chemical disorder, i.e., random distribution of cations with different size and charge (Bi^{3+}, Ba^{2+}) and (Mg^{2+}, Ti^{4+}, Sc^{3+}), on equivalent lattice sites.[6,9,15–17] The temperature of maximum permittivity (T_m) increased with increase in x, probably due to an increase in compositional disorder. The stability of the relative permittivity as a function of temperature increased with increase in x from 0.4 to 0.55 (Table I), and optimum dielectric properties were observed for the sample with x = 0.55, i.e., ε_r = 1430 (±15% in the temperature range of 127°C to 500°C) and tan δ of ≤0.025 over the temperature range of 150°C to 370°C.

Ferroelectric ceramics are typically characterized by measurements at fixed frequency (1 kHz). For better understanding of the dielectric loss and relative permittivity, measurements at variable

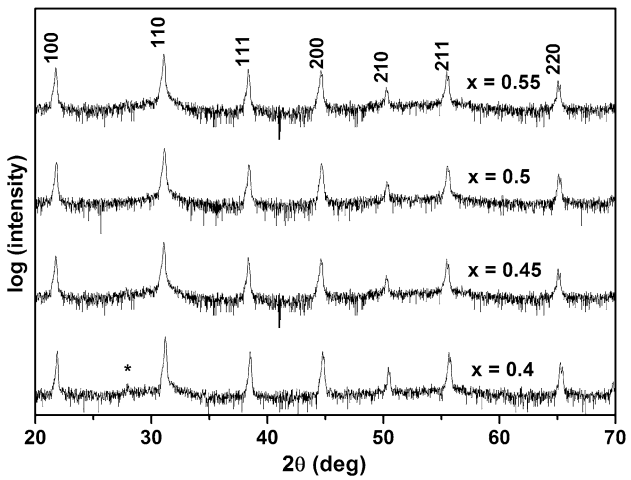

Fig. 1. XRD patterns of BT–BMT–BS, showing formation of single-phase cubic perovskite for samples with $x \ge 0.45$, and an unknown (?) peak for the composition with x = 0.4.

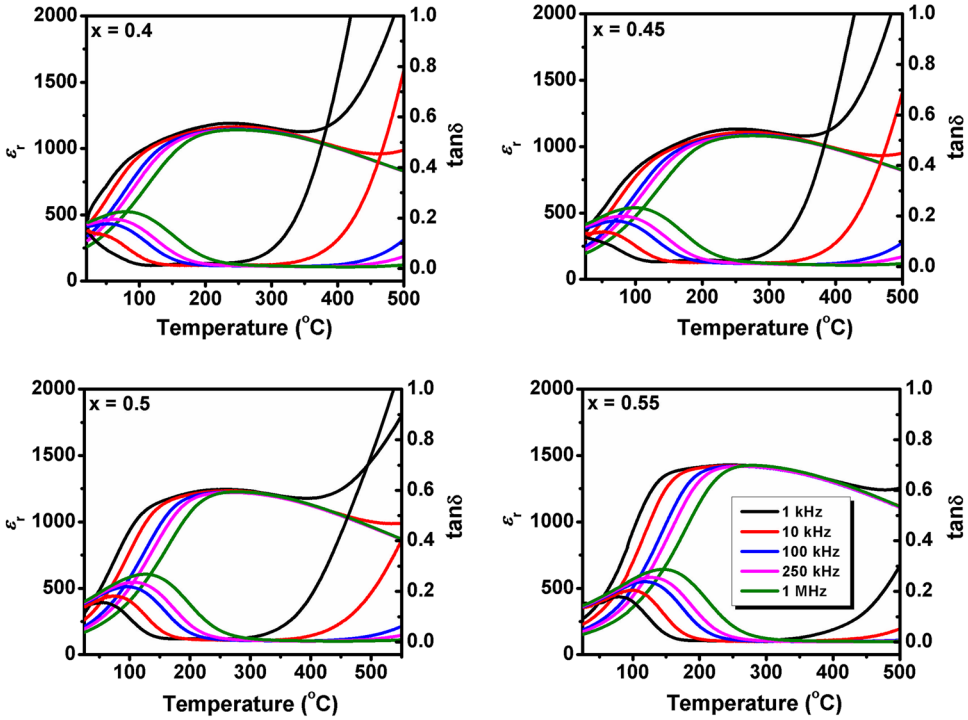

Fig. 2. ε_r and tan δ of BT–BMT–BS as functions of temperature.

Table I. ε_r, tan δ, and their operating temperature ranges for BT–BMT–BS

Sample	$\varepsilon_r \pm 15\%$ (1 kHz)	T Range (°C) $\varepsilon_r \pm 15\%$ (1 kHz)	T Range (°C) tan $\delta < 0.025$ (1 kHz)
$x = 0.40$	1190	110–425	87–245
$x = 0.45$	1140	140–430	113–255
$x = 0.50$	1250	120–495	137–314
$x = 0.55$	1430	127–500	150–370

frequency give information about its origin (intrinsic/extrinsic). Therefore, impedance spectroscopy is a useful technique to investigate the electrical properties of grains and grain boundaries. The resistance (R) and capacitance (C) of an electrical response can be represented by an equivalent circuit. BT-based ceramics usually consist of bulk and grain boundary regions which can be represented by two parallel RC elements connected in series.[18] Each RC element gives a semicircle in the Nyquist plot (Z^*) and electric modulus (M^*), and a Debye peak in spectroscopic plots (Z'' and M''/ε_0 versus log f). Z^* complex-plane plots (Z' versus Z'') of the samples with $x = 0.40$ to 0.55 are shown in Fig. 3, revealing more than one semicircle which are overlapped, indicative of an electrically heterogeneous character. According to the relationship by Ervine et al.,[19] the low-frequency arc corresponds to grain boundary while the high-frequency arc corresponds to bulk. In oxides with ionically or electronically conducting grains, grain boundaries are generally more resistive than grain interiors.[20] The Nyquist plot for the sample with $x = 0.4$ shows three arcs, each indicating an electroactive region, but the highly resistive component is bulk, which is in contradiction to the general relationship. This result shows that the grain boundary is more conductive than the grain, which may be due to presence of impurities within the grain boundaries, consistent with the present XRD data (Fig. 1). Therefore, the boundary region dominates and electrical conduction takes place primarily through the boundaries. The temperature-dependent resistivity of samples indicated semiconducting behavior, which may be due to an increase in the migration of charge carriers, a typical characteristic of material with negative temperature coefficient of resistivity. As x was increased from 0.4 to 0.55, the height of the semicircular arc corresponding to grain boundary (higher frequency) increased, indicating an increase in the resistivity of grain boundary (Fig. 3). The third overlapped arc towards lowest frequency can be attributed to the sample–

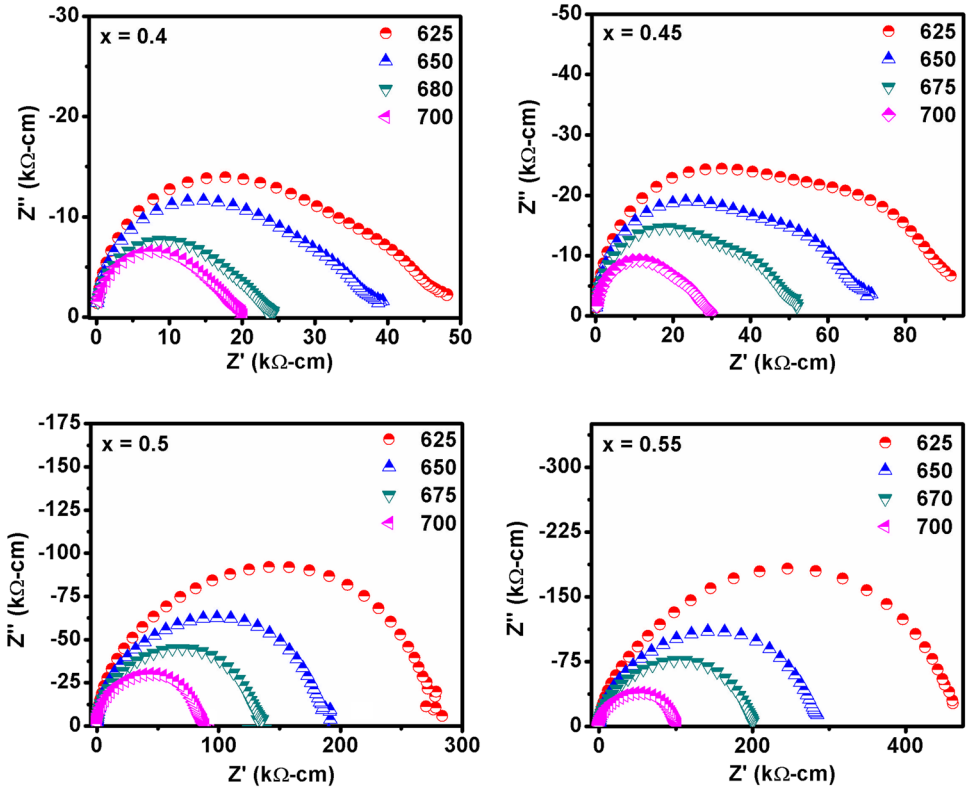

Fig. 3. Nyquist plots of BT–BMT–BS system.

electrode (space charge) effect, almost disappearing for the sample with $x = 0.55$. Generally, the electrode effect is very small in insulating samples, consistent with the present resistance data (Table II).

To further confirm the observed change in resistivity of grain boundary, the combined Z'' and M''/ε_0 versus log f plots were used (Fig. 4). The resistance of bulk and grain boundary was extracted using the following equations:

$$R = 2Z'' \tag{1}$$

$$R = \frac{1}{2\pi \times f_{\max(Z'')} C}. \tag{2}$$

The resistivity, conductivity, and capacitance values of the samples at 600°C are given in Table II, which shows an increase in resistivity with increase in BMT and BS content. Similarly, a decrease in capacitance was also observed, where C_{gb} (in nF) and $C_b \sim 10^{-10}$ F to 10^{-11} F are the capacitance values corresponding to grain boundary and bulk ferroelectric, respectively.[19]

The bulk (σ_b) and grain-boundary conductivity (σ_{gb}) were observed to decrease with increase in x. Arrhenius plots of conductivity for the BT–BMT–BS samples as a function of temperature are shown in Fig. 5. The conductivity is represented by Eq. 3.

$$\sigma = \sigma_0 e^{\frac{-E_a}{k_B T}}, \tag{3}$$

where σ_0 is the preexponential factor, E_a is the activation energy, and k_B is the Boltzmann constant.

The activation energies of bulk and grain boundary were calculated from the slope of conductivity plots (Table II). The activation energies of bulk did not change significantly (0.88 eV to 0.93 eV) with increase in x, suggesting that the bulk conduction mechanism did not change with x. In ferroelectric perovskites, the charge carriers are usually oxygen vacancies.[21] Bi^{3+} has low melting point and exhibits a volatile nature, therefore, during the sintering process, Bi^{3+} may evaporate, which is compensated by creation of oxygen vacancies. Oxygen vacancies are also produced due to escape of oxygen from the host lattice, which can be controlled in an oxidizing environment.[22] A stoichiometric ABO_3 perovskite has $E_a \geq 2$ eV, while the value of E_a is 1 eV for $ABO_{2.95}$ and 0.5 eV for $ABO_{2.90}$.[23] The present activation energies of bulk suggest that oxygen vacancies are responsible for the conduction in BT–BMT–BS. On the other hand, the activation energy of grain boundary increased from 1.12 eV to 1.66 eV (Table II). A similar effect was previously reported for $BaTiO_3$–$Bi(Zn_{1/2}Ti_{1/2})O_3$ ceramics.[16] The data clearly suggest that grain boundary is the main influencing factor that controls the conduction mechanism in the BT–BMT–BS system. However, it is not clear at the present stage whether the minor secondary phase still exists at $x = 0.45$ or not, which is

Table II. Activation energy, resistivity, and capacitance of bulk and grain boundary for BT–BMT–BS samples at 600°C

Sample	E_g (eV)	E_{gb} (eV)	ρ_g (kΩ cm)	ρ_{gb} (kΩ cm)	C_g (pF)	C_{gb} (nF)
x = 0.40	0.88	1.12	35	20	66	3
x = 0.45	0.93	1.29	51	62	94	1.8
x = 0.50	0.88	1.30	87	265	91	0.3
x = 0.55	0.90	1.66	169	806	114	0.22

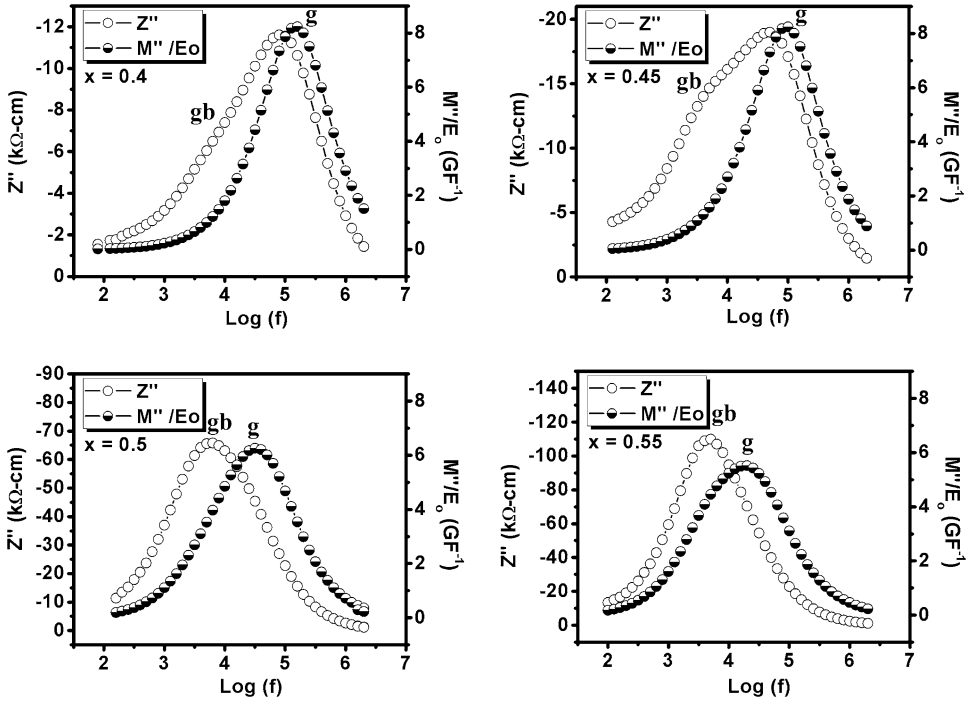

Fig. 4. Z' and M''/ε_0 versus log f plots of BT–BMT–BS at 650°C.

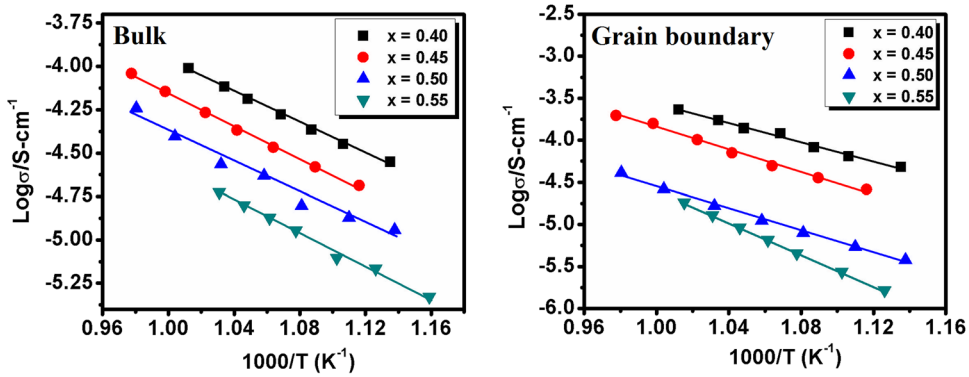

Fig. 5. Arrhenius plot of bulk and grain-boundary conductivity data of BT–BMT–BS as a function of temperature.

worthy of further investigation using transmission electron microscopy to understand the defect chemistry of BT–BMT–BS. Furthermore, control of oxygen vacancies in oxidizing environment may decrease the leakage current and hence the dielectric loss for the sample with x = 0.55, which may be a suitable candidate material for high-temperature applications.

CONCLUSIONS

Lead-free BT–BMT–BS samples were prepared through a conventional mixed-oxide route. Phase analysis revealed formation of an unknown secondary phase for the sample with $x = 0.4$, while single-phase cubic perovskite formed for the samples with $x \geq 0.45$ within the in-house XRD facility detection limit. Impedance spectroscopy of the samples indicated more than one electroactive region, corresponding to an electrically heterogeneous character due to the existence of different transport mechanisms. The activation energies of bulk (0.88 eV to 0.93 eV) suggested conduction due to generation of oxygen vacancies (ionic conduction). However, the activation energy of grain boundary was observed to increase from 1.12 eV to 1.66 eV, which significantly affected the overall conductivity of the sample and hence the dielectric loss. The sample with $x = 0.55$ exhibited a temperature-stable ε_r of $\sim$1430 ($\pm$15% in the operating range of 127°C to 500°C) with tan $\delta < 0.025$ (150°C to 370°C), which may be useful for high-temperature capacitor applications.

ACKNOWLEDGEMENT

The authors thank the Higher Education Commission (HEC) of Pakistan for a research fellowship at the University of Sheffield, UK.

REFERENCES

1. D.S. Tinberg and S. Trolier-McKinstry, *J. Appl. Phys.* 101, 024112 (2007).
2. R.E. Cohen, *Nature* 358, 136 (1992).
3. Y. Yuan, S.R. Zhang, X.H. Zhou, B. Tang, and B. Li, *J. Electron. Mater.* 38, 706 (2009).
4. P. Hagler, P. Henson, and R.W. Johnson, *IEEE Trans. Ind. Electron.* 58, 2673 (2011).
5. M.M. Vijatovic, J.D. Bobic, and B.D. Stojanovic, *Sci. Sinter.* 40, 235 (2008).
6. H. Ogihara, C.A. Randall, and S. Trolier-McKinstry, *J. Am. Ceram. Soc.* 92, 1719 (2009).
7. F. Zhu, M.B. Ward, T.P. Comyn, A.J. Bell, and S.J. Milne, *IEEE Trans. Ultrason. Ferroelectr.* 58, 1811 (2011).
8. R. Dittmer, W. Jo, D. Damjanovic, and J. Rödel, *J. Appl. Phys.* 109, 034107 (2011).
9. B. Xiong, H. Hao, S. Zhang, H. Liu, and M. Cao, *J. Am. Ceram. Soc.* 94, 3412 (2011).
10. Q. Zhang, Z. Li, F. Li, Z. Xu, and S. Zhang, *J. Am. Ceram. Soc.* 94, 4335 (2011).
11. X. Chen, J. Chen, D. Ma, L. Fang, and H. Zhou, *Ceram. Int.* 41, 2081 (2015).
12. A. Zeb, Y. Bai, T. Button, S.J. Milne, and W. Jo, *J. Am. Ceram. Soc.* 97, 2479 (2014).
13. R.D. Shannon, *Acta Crystallogr. Sect. A* 32, 751 (1976).
14. D. Ma, X. Chen, G. Huang, J. Chen, H. Zhou, and L. Fang, *Ceram. Int.* 41, 7157 (2015).
15. H. Ogihara, C.A. Randall, and S. Trolier-McKinstry, *J. Am. Ceram. Soc.* 92, 110 (2009).
16. N. Raengthon and D.P. Cann, *J. Am. Ceram. Soc.* 95, 1604 (2012).
17. N. Raengthon, T. Sebastian, D. Cumming, I.M. Reaney, D.P. Cann, and J. Roedel, *J. Am. Ceram. Soc.* 95, 3554 (2012).
18. F.D. Morrison, D.C. Sinclair, and A.R. West, *J. Am. Ceram. Soc.* 84, 531 (2001).
19. J.T. Irvine, D.C. Sinclair, and A.R. West, *Adv. Mater.* 2, 132 (1990).
20. M. Shah, M. Nadeem, M. Idrees, M. Atif, and M. Akhtar, *J. Magn. Magn. Mater.* 332, 61 (2013).
21. S. Sen, R.N.P. Choudhary, and P. Pramanik, *Phys. B* 387, 56 (2007).
22. C. Ang, Z. Yu, and L. Cross, *Phys. Rev. B* 62, 228 (2000).
23. M. Ramesh and K. Ramesh, *Int. J. Mod. Phys. B* 29, 1550119 (2015).